Available online at www.sciencedirect.com

SciVerse ScienceDirect

Solar Energy 94 (2013) 240–252

SOLAR ENERGY

www.elsevier.com/locate/solener

Development of an analytical optical method for linear Fresnel collectors

Guangdong Zhu *

Concentrating Solar Power Program, National Renewable Energy Laboratory, 15013 Denver West Parkway, Golden, CO, USA

Received 21 December 2012; received in revised form 25 April 2013; accepted 3 May 2013
Available online 13 June 2013

Communicated by: Associate Editor Robert Pitz-Paal

Abstract

An analytical optical approach—**First**-principle **OPT**ical **I**ntercept **C**alculation (FirstOPTIC)—is developed for the optical performance evaluation of linear Fresnel collectors. Instead of treating all optical error sources as probability distributions and convolving them with the sun shape into an overall beam spread function, FirstOPTIC treats mirror slope error, receiver position error, and collector tracking error as geometric modifications to the collector, as interpreted in laboratory measurements. Calculation of intercept factors is analytically derived through a rigorous mathematical model. It is shown through test cases that FirstOPTIC can provide accurate and fast calculation of collector intercept factors as a function of incidence angle. Finally, FirstOPTIC is used to conduct analysis on the incidence angle modifier (IAM) and indicates that the factorized IAM representation with respect to independent transversal and longitudinal components can be a good approximation but in general underestimates the optical performance of a linear Fresnel collector.

Keywords: Concentrating solar power; Linear Fresnel collector; Solar thermal; Non-imaging optics; Intercept factor; Incidence angle modifier

1. Introduction

Linear Fresnel collectors are one of two viable line-focus concentrating solar power (CSP) technologies, along with parabolic troughs. Solar plants utilizing linear Fresnel technology have been commercially tested and/or deployed on a utility scale around the world (Mills and Morrison, 2000; Zhu et al., 2013). One important aspect of a linear Fresnel collector is its optical performance. Optical performance evaluation often involves optical and/or mechanical characterization of the linear Fresnel collector, including characterizing the mirror specularity and the collector's geometric precision. The sun shape also has an impact on a collector's optical performance, and it varies with time and location. The most common approach to optical performance evaluation is ray tracing. Available ray-tracing software includes specialized codes for CSP applications such as SOLTRACE (Wendelin, 2003) and some general-purpose commercial optical tools like ASAP (Breault Research Organization). Ray tracing generates a set of sun rays simulating the original or broadened/altered sun shape and lets them interact with various collector components with specified optical properties and mechanical aspects. The number of sun rays needs to be large enough to produce results with desired precision, and the computation, in some cases involving complex geometries and/or a large volume of data, can be time consuming.

Very often in ray-tracing approaches, optical error sources resulting from the geometric errors of a linear Fresnel collector, such as mirror surface slope error, receiver position error, and mirror tracking error, are converted into optical errors represented as probability distribution functions. The probability distribution functions of various geometric errors are then convolved with the sun shape and

* Tel.: +1 303 275 4497.
E-mail address: Guangdong.Zhu@nrel.gov

0038-092X/$ - see front matter © 2013 Elsevier Ltd. All rights reserved.
http://dx.doi.org/10.1016/j.solener.2013.05.003

Nomenclature

i	an index
$E_{source\ i}$	the distribution function for a collector optical error source i
g	a general distribution function
g_{eff}	the effective beam spread distribution
g_{sun}	the sun shape
g_{spec}	the mirror specularity profile distribution
μ	the mean value of a distribution
σ	the root mean square of a distribution
μ_{total},σ_{total}	the mean value and the root mean square of the overall beam spread function, mrad
μ_{sun}, σ_{sun}	the mean value and the root mean square of the sun shape distribution, mrad
$\mu_{specularity}$, $\sigma_{specularity}$	the mean value and the root mean square of the reflector specularity distribution, mrad
μ_{slope}, σ_{slope}	the mean value and the root mean square of the reflector slope error distribution, mrad
$\mu_{receiver}$, $\sigma_{receiver}$	the mean value and the root mean square of the receiver position error distribution, mrad
μ_{track}, σ_{track}	the mean value and the root mean square of the collector tracking error distribution, mrad
k	the mirror index
τ^k	the linear Fresnel mirror tracking angle for mirror k
$\theta_{\perp}$	the transversal incidence angle
$\theta_{\parallel}$	the longitudinal incidence angle
θ^k_{aim}	the aiming angle of mirror k in the transversal plane
x	the coordinate along collector width, m or mm
y	the coordinate along collector length, m or mm
z	the coordinate along the normal vector of the collector aperture, m or mm
$\overrightarrow{I_x}$	the unit vector along the x axis
$\overrightarrow{I_y}$	the unit vector along the y axis
$\overrightarrow{I_z}$	the unit vector along the z axis
$\vec{v}$	a general vector
$\overrightarrow{v_i}$	the nominal incoming sun ray vector
$\overrightarrow{v_n}$	the reflected vector on a surface
$\overrightarrow{v_r^+}$	the upper limiting vector of the receiver acceptance angular window
$\overrightarrow{v_r^-}$	the lower limiting vector of the receiver acceptance angular window
$\overrightarrow{v^+}_{blocking}$	the upper limiting vector of the receiver acceptance angular window accounting for the blocking effect
$\overrightarrow{v^-}_{blocking}$	the lower limiting vector of the receiver acceptance angular window accounting for the blocking effect
$\overrightarrow{v^+}_{shading/blocking}$	the upper limiting vector of the receiver acceptance angular window accounting for the blocking and shading effects
$\overrightarrow{v^-}_{shading/blocking}$	the lower limiting vector of the receiver acceptance angular window accounting for the blocking and shading effects
T^+	the upper limiting plane tangent to the receiver tube
T^-	the upper limiting plane tangent to the receiver tube
$\overrightarrow{n_s}$	the surface normal vector
Reft	the reflection function operator
$[RT]$	the rotational matrix (function)
h_r	the receiver assembly height
Δx_r	the receiver position error along x direction, mm
Δz_r	the receiver position error along z direction, mm
ε_x	the transversal slope error
ε_y	the longitudinal slope error
β^+_{ideal}	the ideal upper limit of the receiver acceptance angle window in the transversal plane, mrad
β^+_{ideal}	the ideal lower limit of the receiver acceptance angle window in the transversal plane, mrad
β^+	the upper limit of the receiver acceptance angle window in the transversal plane, mrad
β^-	the lower limit of the receiver acceptance angle window with the slope/tracking errors, mrad
β^+_{3D}	the upper limit of the receiver acceptance angle window in three dimensions, mrad
β^-_{3D}	the lower limit of the receiver acceptance angle window in three dimensions, mrad
∂	the partial differential operator
γ	the collector intercept factor
η	the collector optical efficiency
ρ	the reflector reflectance
τ	the transmittance of the receiver glass envelope
α	the receiver absorptance
IAM	the incidence angle modifier
δ	the Dirac delta function

the mirror specularity so that an effective broadened beam spread cone can be obtained to incorporate all system errors of the collector. However, it has been shown that this error-convolution approach is not accurate in many occasions and is not capable of correctly treating some geometric errors such as receiver position error for trough collectors (Zhu and Lewandowski, 2012; Zhu, 2013), which can also apply to linear Fresnel collectors.

In this paper, an analytical approach called **First**-principle **OPT**ical **I**ntercept **C**alculation (FirstOPTIC) is presented to quickly and accurately evaluate the optical performance of linear Fresnel collectors. FirstOPTIC treats optical error sources in the way they are typically characterized in laboratory measurements using a geometric or optical interpretation (Rabl, 1985). For instance, slope error is measured as a geometric deviation of actual mirror

slope from desired values, so it should be treated as a geometric factor as a function of spatial variables (Wendelin et al., 2006; Andraka et al., 2009; Pottler et al., 2005), instead of a simple optical error distribution uniformly applied to every point on the mirror surface. The latter will result in the loss of spatial dependence in slope error distribution and leads to inaccurate optical evaluation (Zhu and Lewandowski, 2012).

Right now, the only method to evaluate linear Fresnel collector is ray-tracing. The development of such an analytical approach (FirstOPTIC) provides an alternative effective approach for the optical evaluation of linear Fresnel collectors. In addition, FirstOPTIC as an analytical approach will be greatly superior to ray-tracing method in computational speed by reducing the order of computational complexity because: (1) FirstOPTIC traces the rays as a group instead of individual rays and (2) it would be much more accurate and efficient to simulate the interaction between sun rays and reflector surface with various geometrical representations such as mirror slope error. For example, when a reflector is represented by a set of discrete finite elements, FirstOPTIC may be thousands of times faster than a Monte Carlo ray tracing method (Zhu and Lewandowski, 2012). The FirstOPTIC approach would greatly facilitate the optimization of linear Fresnel collectors with respect to a large number of design parameters existing in a linear Fresnel collector design.

The paper is organized as follows. Technical interpretation of linear Fresnel collectors is first described in Section 2; in Section 3, the mathematical model of FirstOPTIC is presented in detail; Section 4 shows the validation of the numerical code of FirstOPTIC; a case study is given to demonstrate the capability of FirstOPTIC in Section 5; and finally, the work in this paper is concluded in Section 6 along with further directions.

2. Technical representation of linear Fresnel collectors

As illustrated in Fig. 1, a linear Fresnel collector uses an array of low-profile, nearly flat primary reflectors and a fixed receiver assembly including one or more linear receiver tubes and an optional secondary reflector. The primary reflectors track the sun in the daytime while the receiver assembly remains fixed. The low-profile reflector architecture allows for a higher concentration ratio without increasing wind loads, which is otherwise the case for parabolic troughs (Price et al., 2002) due to the fact that the wind load is proportional to the square of the mirror aperture and is also a function of height. In addition, the linear nature of this technology may potentially drive lower-cost solar fields and lower-cost maintenance, compared with central-receiver towers (Rabl, 1985; Kolb et al., 2007). Optical analysis of linear Fresnel collectors can be described by two main characteristics: geometry and optics. Commercial linear Fresnel collectors (Bernhard et al., 2008; Conlon, 2011; Barale et al., 2010; Selig, 2011; Morin et al., 2011) often differ in either their specific geometry or optics, but they share the same general geometric and optical attributes. Many of linear Fresnel collectors employ secondary reflector as part of the fixed receiver assembly to increase the collector optical efficiency, but there also exist some arguments that secondary reflectors may not be economically justified with respect to extra cost and additional operation/maintenance efforts when the receiver size increases (Mills and Morrison, 2000; Brost and Zhu, 2009; Brost and Zhu, 2010). In particular, when multiple receiver tubes are used, the optical benefits resulting from the secondary reflector may be minimal and additional component cost related to the secondary reflector may not justify its usage (Mills and Morrison, 2000). In addition, a single large-size receiver may also help improving the collector optical performance, reducing the plant parasitic on the HTF pumping in the field and avoiding the additional maintenance work required for the secondary reflector (Brost and Zhu, 2009; Brost and Zhu, 2010). There is also a tendency to combine photovoltaic cells with linear Fresnel receiver assembly to increase the collector efficiency instead of using the secondary reflector. Thus, linear Fresnel without secondary reflectors certainly has its value in the industrial applications and obtains more and more attentions.

In the scope of work here, FirstOPTIC is developed for linear Fresnel collectors without secondary reflectors. Although the secondary reflector is often used, there is no consensus on its optimum shape. Many secondary reflector geometries have been proposed throughout the literature including the compound parabolic shape, the trapezoidal shape and the flat parabolic shape (Zhu et al., 2013). Due to the numerical difficulties addressing the arbitrary geometries of secondary reflectors, the incorporation of secondary reflectors into FirstOPTIC will be addressed in the future work.

2.1. Geometric aspects

Simplified schematics of a generic linear Fresnel collector are given in Fig. 1. The incidence angle is defined as the angle between the reference direction of a collector and the nominal direction of incoming sun rays. For linear Fresnel collectors, the reference direction used to define the incidence angle(s) is conventionally chosen to be the zenith axis (i.e., normal incidence). The incidence angle is split into angles in two planes: the transversal plane and the longitudinal plane, which are perpendicular and parallel to the linear axis of linear Fresnel reflectors (y axis), respectively. Thus, the sun position can also be represented by a combination of transversal and longitudinal incidence angles, $(\theta_{\perp}, \theta_{\parallel})$.

Geometrically, a linear Fresnel collector is defined by a variety of parameters, including:

- number of mirror rows,
- mirror spacing,
- mirror shape,

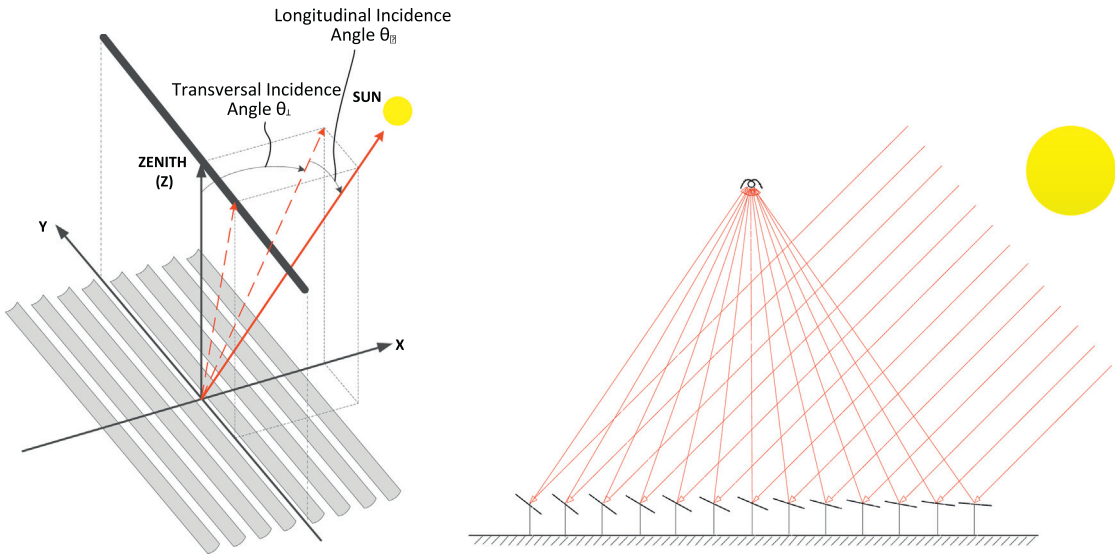

Fig. 1. Schematics of a generic linear Fresnel collector.

– mirror height,
– mirror width,
– receiver assembly height,
– receiver assembly size,
– receiver assembly geometry,
– collector unit/loop length.

All of the above geometric parameters may vary from one collector to another. It is extremely challenging to optimize a linear Fresnel collector with respect to most or all of the relevant parameters, especially when coupled with the collector's optical properties. In most cases, one starts with an empirical baseline linear Fresnel design and optimizes the very few selected parameters considered most important to the overall optical and/or economic performance (Zhu et al., 2013).

2.2. Optical aspects

Both the optical properties and mechanical precisions of the collector components affect the optical performance of a collector and could be optical error sources; these include mirror specularity (Pettit, 1977; Meyen et al., 2013; Gee et al., 2010; Bendt et al., 1979), mirror slope error, receiver position error, and collector tracking error. The treatment of the sun shape and all optical error sources varies depending on the specific needs of the collector optical characterization. Conveniently, all optical error sources may be treated or approximated by probability distributions and then convolved into an overall probability distribution representing an effective beam spread cone.

Assuming the sun shape and error sources are characterized by a probability distribution function:

$$E_{source\ i} = g_i(\beta). \tag{1}$$

Here, β is the angular value measured from the nominal direction, and i stands for each specific error source. Then an effective error cone can be obtained by convolving all error distributions and the sun shape to formulate the overall beam spread. The overall beam spread accounting for the sun shape and all system optical errors may be represented by an overall probability function:

$$B_{total} = g_{total}(\beta). \tag{2}$$

When the sun shape and all optical sources are a simple Gaussian as suggested by Bendt et al. (1979), the overall convolved beam spread will be a simple Gaussian as well: its mean value (μ_{total}) is simply the summation of the mean value of each individual profile and its root mean square (RMS) value is the quadratic mean of the RMS of each individual profile (Boas, 1983). Namely:

$$\mu_{total} = \mu_{sun} + \mu_{specularity} + 2\mu_{slope} + \mu_{receiver} + 2\mu_{track}; \tag{3}$$

$$\sigma^2_{total} = \sigma^2_{sun} + \sigma^2_{specularity} + (2\sigma_{slope})^2 + \sigma^2_{receiver} + (2\sigma_{track})^2. \tag{4}$$

Here,

μ_{sun}, σ_{sun}: mean value and RMS of the sun shape distribution,
$\mu_{specularity}$, $\sigma_{specularity}$: mean value and RMS of the reflector specularity distribution,
μ_{slope}, σ_{slope}: mean value and RMS of the reflector slope error distribution,
$\mu_{receiver}$, $\sigma_{receiver}$: mean value and RMS of the receiver position error distribution,
μ_{track}, σ_{track}: mean value and RMS of the collector tracking error distribution.

The factor of 2 for some of the error sources above comes from the fact that, starting from a straightforward yet strict geometric analysis based on the linear Fresnel

geometries, any angular variation in each of these relevant error sources would result in twice the angular variation in the overall beam spread because of the reflection law.

Though the probability approximation approach has been widely used in some ray-tracing programs, it results in an inaccurate evaluation of a collector's optical performance. First, the probability approximation approach loses spatial dependence of the mirror slope error and the receiver position error by using a probability approximation as a direct convolution with other error sources. Second, when using a simple Gaussian, the probability approximation approach does not account for the systematic effects of the mirror slope error, the receiver position error, and the tracking error (Brost and Zhu, 2009). Very often, one needs to build each individual error source into ray-tracing software in a very sophisticated way to more accurately assess a collector's optical performance.

This paper proposes an alternative and more accurate approach to treat the errors for linear Fresnel collectors in the way they are typically characterized in laboratory measurements using a geometric or optical interpretation.

3. Mathematical model of FirstOPTIC

FirstOPTIC is an analytical approach to perform optical analysis of concentrating collectors. It employs appropriate optical treatment of collector optical error sources and derives analytical mathematical formulae to calculate the intercept factor of a concentrating solar collector (Rabl, 1985; Bendt et al., 1979). The intercept factor is defined as the ratio of solar power intercepted by the receiver to the solar power intercepted by the total collector aperture. Mirror slope error, receiver position error, and mirror tracking error are traditionally measured as geometric modifications to the collector and should be treated as the geometric factors of the collector, and equivalent probability distribution representations exist only in some special scenarios. For instance, at normal incidence, a tracking error at a particular moment is mathematically equivalent to imposing the same angular offset to the originating beam relative to the receiver for a linear Fresnel collector. The overall tracking error incorporating temporal effect can then be accounted for precisely as a probability distribution by direct convolution with the originating sun beam.

FirstOPTIC has been successfully developed for parabolic trough collectors by Zhu and Lewandowski (2012). Here, FirstOPTIC is extended to linear Fresnel collectors. This section presents the detailed mathematical model of FirstOPTIC to calculate the intercept factors of linear Fresnel collectors.

3.1. Effective beam spread

When sun rays are reflected on mirror surfaces, the sun shape is effectively broadened or altered by mirror specularity. For a linear Fresnel collector, an effective beam spread function, including the sun shape and the mirror specularity, can then be defined as a probability function:

$$B_{eff} = g_{eff}(\beta) = (g_{sun} * g_{spec})(\beta). \tag{5}$$

Here, $g_{sun}(\beta)$ and $g_{spec}(\beta)$ are the probability distribution profiles of the sun shape and mirror specularity, respectively. In addition:

$$\int_{-\infty}^{+\infty} g_{eff}(\beta)d\beta = 1. \tag{6}$$

The effective beam spread may also include other types of optical error sources when needed, as seen in Eqs. (2)–(4). In FirstOPTIC, the other optical error sources, such as mirror slope error, receiver position error, and mirror tracking error, are typically treated as geometric modifications to the collector, as shown next.

3.2. Modular configuration

Linear Fresnel reflectors track the sun over time, and each mirror suffers from shading and blocking from neighboring mirrors, as shown in Fig. 2. Shading of a mirror is blockage of incoming sun rays reaching the mirror by its neighbor(s), and blocking is blockage of reflected sun rays reaching the receiver assembly by its neighbor(s). One observation for linear Fresnel reflectors is that the optical performance of a mirror can typically be derived from its local configuration involving only the mirror itself, its neighboring mirrors, and the receiver assembly, and is independent of the rest of mirrors within a collector. Thus, the overall optical performance of a linear Fresnel collector can then be obtained by separating it into a modular calculation of a three-mirror configuration, or a two-mirror configuration for the outermost mirrors. It is true that shading of neighboring collectors may occur at high incidence angles, but its impact is neglected in the proposed analytical method here.

3.3. Mirror tracking angle

For a mirror k in a linear Fresnel reflector array shown in Fig. 3, the tracking angle is defined as $\boldsymbol{\tau^k}$ for a sun position represented by the transversal and longitudinal incidence angles $(\boldsymbol{\theta}_{\perp}, \boldsymbol{\theta}_{\parallel})$ as shown in Fig. 1. To calculate $\boldsymbol{\tau_k}$, first assume: the pivot point of the mirror k, $(\boldsymbol{x_0^k}, \boldsymbol{z_0^k})$; the collector aiming point, (x_{aim}, z_{aim}), which may or may not be the center of the receiver assembly $(0, h_r)$; and the angular position of the sun in the transversal plane, $\boldsymbol{\theta}_{\perp}$. Then the tracking angle can be determined as follows:

$$\tau^k = \frac{\left(\theta^k_{aim} + \theta_{\perp}\right)}{2}, \tag{7}$$

Where:

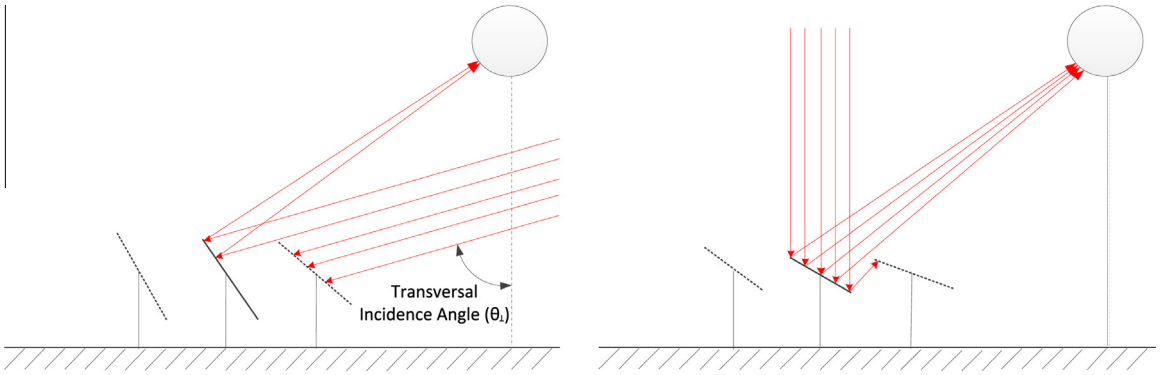

Fig. 2. Shading (left) and blocking (right) for a linear Fresnel collector's geometric formation.

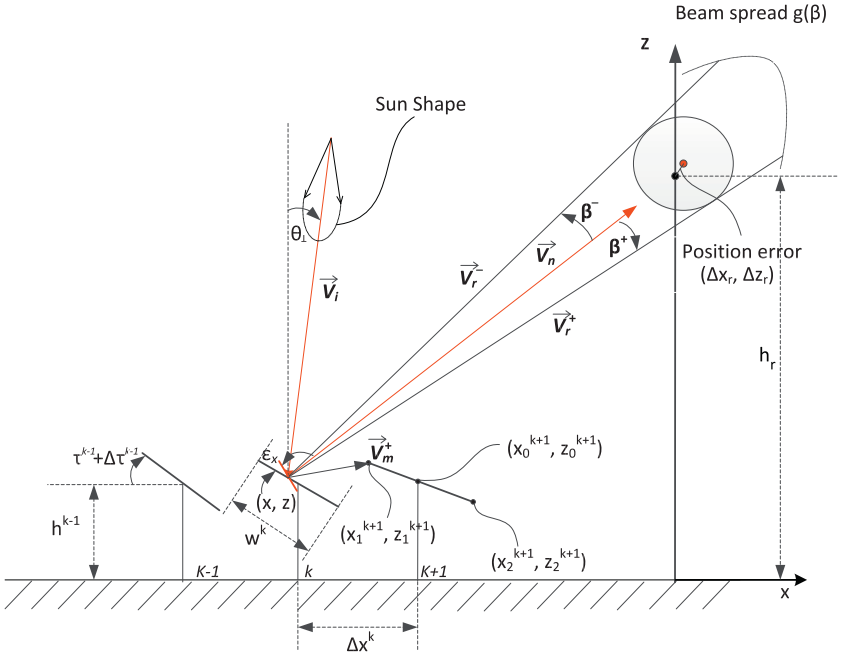

Fig. 3. Illustration of receiver acceptance angle calculation.

$$\theta_{aim}^{k} = \frac{\left(\overrightarrow{I_z} \times \overrightarrow{v_{aim}^{k}}\right)_y}{\left|\left(\overrightarrow{I_z} \times \overrightarrow{v_{aim}^{k}}\right)_y\right|} \cdot \arccos\left(\frac{\overrightarrow{I_z} \cdot \overrightarrow{v_{aim}^{k}}}{\left|\overrightarrow{I_z}\right| \cdot \left|\overrightarrow{v_{aim}^{k}}\right|}\right); \tag{8}$$

$$\overrightarrow{I_z} = \begin{Bmatrix} 0 \\ 0 \\ 1 \end{Bmatrix}; \quad \overrightarrow{v_{aim}^{k}} = \begin{Bmatrix} x_{aim} - x_0^k \\ 0 \\ z_{aim} - z_0^k \end{Bmatrix}. \tag{9-10}$$

3.4. Calculation of acceptance angles within the transversal plane

As shown in Fig. 3, the collector is sketched in the transversal plane. For a point (x,z) of interest, the transversal slope error ε_x is the angular deviation at this particular point from its desired slope within the transversal plane. It is a function of spatial variables. The desired receiver position is at $(0,h_r)$ and the associated receiver position error is defined $(\Delta x_r, \Delta z_r)$. The angular tracking error is then treated as an offset to the tracking angle of the mirror k, $\Delta\tau^k$. All notations can be naturally extended to all mirrors for a collector. The shape of the mirrors can be flat, circular, or parabolic. As shown here, the mirror slope error, the receiver position error, and the collector tracking error are incorporated as the geometric attributes of a linear Fresnel collector.

The receiver acceptance angle window (upper limit β^+, lower limit β^-) is also often used in the optical analysis (Zhu and Lewandowski, 2012; Bendt et al., 1979; Rabl, 1976) and is defined as the angular range of beam spread distribution within which the sun rays would be intercepted by the receiver. This section demonstrates a procedure to calculate the receiver acceptance angle window limits within the transversal plane.

First, the nominal incoming sun direction is defined by its transversal incidence angle, $\theta_\perp$:

$$\overrightarrow{v_i} = \begin{Bmatrix} \sin(\theta_\perp) \\ \cos(\theta_\perp) \\ 0 \end{Bmatrix}. \tag{11}$$

Then its reflected vector $\overrightarrow{v_n}$ at the surface point (x,z) is:

$$\overrightarrow{v_n} = \mathrm{Reft}(\overrightarrow{v_i}, \overrightarrow{n_s}) = (2 \cdot |\overrightarrow{v_i} \cdot \overrightarrow{n_s}|)\overrightarrow{n_s} - \overrightarrow{v_i}, \tag{12}$$

where $\overrightarrow{\boldsymbol{n}_s}$ is the surface normal vector at (x,z) and can be calculated as:

$$\overrightarrow{n_s} = [RT_{xz}(\tau^k + \Delta\tau^k + \varepsilon_x)] \cdot \overrightarrow{n_0}; \tag{13}$$

$$\overrightarrow{n_0} = \begin{Bmatrix} -z(x)' \\ 0 \\ 1 \end{Bmatrix}. \tag{14}$$

For convenience, a function $\mathbf{Reft}(\vec{\boldsymbol{v}}, \vec{\boldsymbol{n}})$ is defined to calculate the reflection of a vector $\vec{\boldsymbol{v}}$ with respect to a surface normal vector $\vec{\boldsymbol{n}}$.

In addition, $[\boldsymbol{RT}_{xz}(\boldsymbol{\theta})]$ is the rotational matrix, which rotates a vector around axis y within the xz plane by an angle θ. It is defined as:

$$[RT_{xz}(\theta)] = \begin{bmatrix} \cos(\theta) & 0 & -\sin(\theta) \\ 0 & 1 & 0 \\ \sin(\theta) & 0 & \cos(\theta) \end{bmatrix}. \tag{15}$$

Next, the acceptance angle limits at the surface point (x,z) without considering shading and blocking can be calculated as:

$$\beta^{+,k}_{ideal}(x,z) = \arccos\left(\frac{\overrightarrow{v_r^+} \cdot \overrightarrow{v_n}}{|\overrightarrow{v_r^+}| \cdot |\overrightarrow{v_n}|}\right);$$

$$\beta^{-,k}_{ideal}(x,z) = \arccos\left(\frac{\overrightarrow{v_r^-} \cdot \overrightarrow{v_n}}{|\overrightarrow{v_r^-}| \cdot |\overrightarrow{v_n}|}\right). \tag{16-17}$$

Here, $\overrightarrow{\boldsymbol{v}_r^+}$ and $\overrightarrow{\boldsymbol{v}_r^-}$ are the vectors emanating from (x,z) and tangent to the receiver outer surface, as shown in Fig. 3:

$$\overrightarrow{v_r^+} = [RT_{xz}(\varphi)] \cdot \overrightarrow{v_c}; \quad \overrightarrow{v_r^-} = [RT_{xz}(-\varphi)] \cdot \overrightarrow{v_c}; \tag{18-19}$$

$$\overrightarrow{v_c} = \begin{Bmatrix} \Delta x_r - x \\ 0 \\ h_r + \Delta z_r - z \end{Bmatrix}; \tag{20}$$

$$\varphi = \arcsin\left(\frac{d/2}{|\overrightarrow{v_c}|}\right), \text{ for a circular receiver.} \tag{21}$$

When blocking from neighboring mirrors is taken into account, the limiting vectors $\overrightarrow{\boldsymbol{v}_r^+}$ and $\overrightarrow{\boldsymbol{v}_r^-}$ need to be modified as:

$$\overrightarrow{v^+}_{blocking} = \begin{cases} \overrightarrow{v_r^+}, & if \left(\overrightarrow{v_r^+} \times \overrightarrow{v_m^+}\right)_y > 0; \\ \overrightarrow{v_m^+}, & if \left(\overrightarrow{v_r^+} \times \overrightarrow{v_m^+}\right)_y \leqslant 0. \end{cases} \tag{22}$$

And

$$\overrightarrow{v^-}_{blocking} = \begin{cases} \overrightarrow{v_r^-}, & if \left(\overrightarrow{v_r^-} \times \overrightarrow{v_m^-}\right)_y < 0; \\ \overrightarrow{v_m^-}, & if \left(\overrightarrow{v_r^-} \times \overrightarrow{v_m^-}\right)_y \geqslant 0. \end{cases} \tag{23}$$

Here, $\overrightarrow{v_m^+}$ and $\overrightarrow{v_m^-}$ are the vectors emanating from (x,z) to the left end of the mirror on the right (mirror $k+1$) and the right end of the mirror on the left (mirror $k-1$), respectively, as shown in the figure:

$$\overrightarrow{v_m^+} = \begin{Bmatrix} x_1^{k+1} - x \\ 0 \\ z_1^{k+1} - z \end{Bmatrix}; \quad \overrightarrow{v_m^-} = \begin{Bmatrix} x_2^{k-1} - x \\ 0 \\ z_2^{k-1} - z \end{Bmatrix}. \tag{24-25}$$

To be more specific, the ends of each mirror k can be calculated as:

$$x_1^k = x_0^k - \frac{w^k}{2} \cdot \cos(\tau^k); \quad z_1^k = z_0^k + \frac{w^k}{2} \cdot \sin(\tau^k); \tag{26-27}$$

$$x_2^k = x_0^k + \frac{w^k}{2} \cdot \cos(\tau^k); \quad z_1^k = z_0^k - \frac{w^k}{2} \cdot \sin(\tau^k). \tag{28-29}$$

Here, w^k is the width of the mirror k.

In addition, when shading from neighboring mirrors is taken into account, the limiting vectors need to be updated again:

$$\overrightarrow{v^+} = \overrightarrow{v^+}_{shading/blocking} = \begin{cases} \overrightarrow{v^+}_{blocking}, & if \left(\overrightarrow{v^+}_{blocking} \times \overrightarrow{v^+_{m,\,reflection}}\right)_y > 0; \\ \overrightarrow{v^+_{m,\,reflection}}, & if \left(\overrightarrow{v^+}_{blocking} \times \overrightarrow{v^+_{m,\,reflection}}\right)_y \leqslant 0. \end{cases} \tag{30}$$

And

$$\overrightarrow{v^-} = \overrightarrow{v^-}_{shading/blocking} = \begin{cases} \overrightarrow{v^-}_{blocking}, & if \left(\overrightarrow{v^-}_{blocking} \times \overrightarrow{v^-_{m,\,reflection}}\right)_y < 0; \\ \overrightarrow{v^-_{m,\,reflection}}, & if \left(\overrightarrow{v^-}_{blocking} \times \overrightarrow{v^-_{m,\,reflection}}\right)_y \geqslant 0. \end{cases} \tag{31}$$

Here, $\overrightarrow{v^+_{m,\,reflection}}$ and $\overrightarrow{v^-_{m,\,reflection}}$ are the respective reflections of $\overrightarrow{v_m^+}$ and $\overrightarrow{v_m^-}$ with respect to the local surface normal $\overrightarrow{n_s}$:

$$\overrightarrow{v^+_{m,\,reflection}} = Reft\left(\overrightarrow{v_m^-}, \overrightarrow{n_s}\right);$$

$$\overrightarrow{v^-_{m,\,reflection}} = Reft\left(\overrightarrow{v_m^+}, \overrightarrow{n_s}\right); \tag{32-33}$$

At last, the acceptance angle limits at the surface point (x,z) taking into account shading and blocking can be calculated as:

$$\beta^{+,k}(x,z) = \arccos\left(\frac{\overrightarrow{v^+} \cdot \overrightarrow{v_n}}{|\overrightarrow{v^+}| \cdot |\overrightarrow{v_n}|}\right);$$

$$\beta^{-,k}(x,z) = \arccos\left(\frac{\overrightarrow{v^-} \cdot \overrightarrow{v_n}}{|\overrightarrow{v^-}| \cdot |\overrightarrow{v_n}|}\right). \tag{34-35}$$

Though the acceptance angles are derived for a circular receiver here, a similar procedure can be followed for other types of receiver assemblies, as well. Eq. (21) would vary with the shape/configuration of the receiver assembly used. The derivation of the acceptance angles involving a secondary reflector is also straightforward but would involve more computational effort.

3.5. Calculation of acceptance angles in three dimensions

In three dimensions, the sun position is represented by both the transversal and longitudinal incidence angles, ($\theta_\perp$, $\theta_\parallel$), and the acceptance angle can be derived using a similar procedure—but some vectors in the previous section need to be extended or re-derived. As shown in Fig. 4, the longitudinal slope error ε_y is added to a mirror surface in three dimensions.

First of all, the nominal incoming sun ray vector $\overrightarrow{v_i}$ becomes:

$$\overrightarrow{v_i} = \begin{Bmatrix} \cos(\theta_\parallel)\sin(\theta_\perp) \\ \cos(\theta_\parallel)\cos(\theta_\perp) \\ \sin(\theta_\parallel) \end{Bmatrix}; \tag{36}$$

For a surface point (x, y, z) on the mirror k, the normal vector will be with the tracking error $\Delta\tau^k$ and transversal and longitudinal slope errors ε_x and ε_y:

$$\overrightarrow{n_s} = \left[RT_{yz}\left(\varepsilon'_y\right)\right] \cdot \left[RT_{xz}(\tau^k + \Delta\tau^k + \varepsilon_x)\right] \cdot \overrightarrow{n_0}; \tag{37}$$

where

$$\varepsilon'_y = \arctan(\tan(\varepsilon_y)\cos(\varepsilon_x)). \tag{38}$$

Then, the reflection of the nominal incoming sun ray $\overrightarrow{v_i}$ at this surface point is:

$$\overrightarrow{v_n} = \mathrm{Reft}(\overrightarrow{v_i}, \overrightarrow{n_s}). \tag{39}$$

The normal vector to the incoming sun ray plane ***S***, which includes the nominal sun vector $\overrightarrow{v_i}$ and the unit vector $\overrightarrow{I_x}$ along the x axis, is then:

$$\overrightarrow{n_i} = \frac{\overrightarrow{v_i} \cdot \overrightarrow{I_x}}{|\overrightarrow{v_i} \cdot \overrightarrow{I_x}|}. \tag{40}$$

The normal to the reflection plane **R** is then:

$$\overrightarrow{n_r} = \mathrm{Reft}(\overrightarrow{n_i}, \overrightarrow{n_s}). \tag{41}$$

To calculate the limiting vectors $\overrightarrow{v^+_{r,3D}}$ and $\overrightarrow{v^-_{r,3D}}$, the limiting planes T^+ and T^-, which originate from the surface point of interest $P(x, y, z)$ and are tangent to the receiver, are defined. The normal vectors to the planes T^+ and T^- are:

$$\overrightarrow{n^+_T} = I_y \times \overrightarrow{v^+_r}; \quad \overrightarrow{n^-_T} = I_y \times \overrightarrow{v^-_r}. \tag{42-43}$$

Then the limiting vectors are:

$$\overrightarrow{v^+_{r,3D}} = \overrightarrow{n^+_T} \times \overrightarrow{n_r}; \quad \overrightarrow{v^-_{r,3D}} = \overrightarrow{n^-_T} \times \overrightarrow{n_r}. \tag{44-45}$$

The neighboring vectors $\overrightarrow{v^+_m}$ and $\overrightarrow{v^-_m}$ are projected to the reflection plane:

$$\overrightarrow{v^+_{m,3D}} = \left(\overrightarrow{v^+_m} \times \overrightarrow{n_r}\right) \times \overrightarrow{n_r}; \quad \overrightarrow{v^-_{m,3D}} = \left(\overrightarrow{v^-_m} \times \overrightarrow{n_r}\right) \times \overrightarrow{n_r}. \tag{46-47}$$

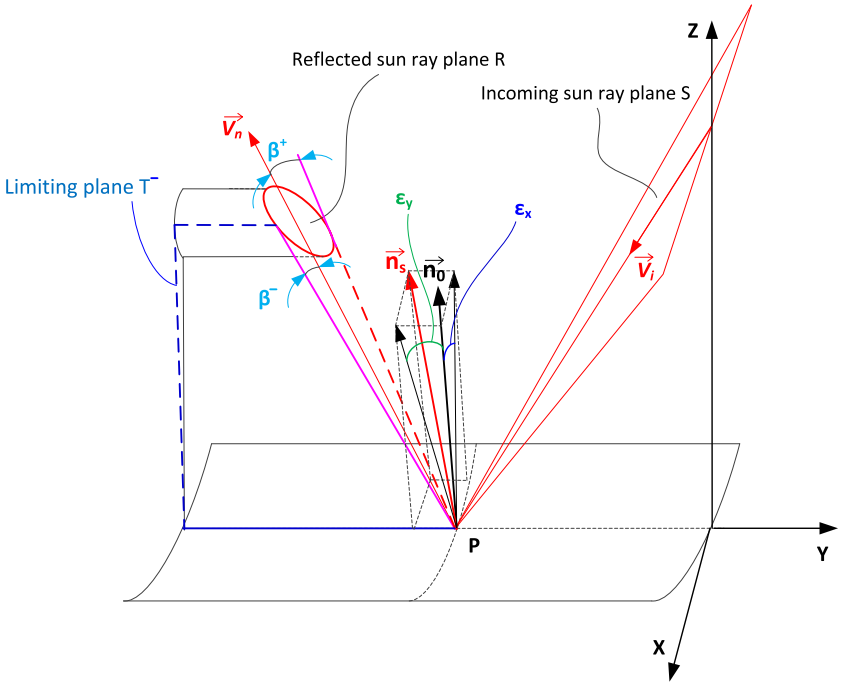

Fig. 4. Illustration of receiver acceptance angle calculation in three dimensions (Binotti et al., 2013).

Thus, the limiting vectors incorporating shading and blocking from the neighboring mirrors are calculated by following the same procedure from Eqs. (22) to (31).

To take into account the blocking:

$$\overrightarrow{v^{+}_{3D,blocking}} = \begin{cases} \overrightarrow{v^{+}_{r,3D}}, & if \left(\overrightarrow{v^{+}_{r,3D}} \times \overrightarrow{v^{+}_{m,3D}}\right) \cdot \overrightarrow{n_r} > 0; \\ \overrightarrow{v^{+}_{m,3D}}, & if \left(\overrightarrow{v^{+}_{r,3D}} \times \overrightarrow{v^{+}_{m,3D}}\right) \cdot \overrightarrow{n_r} \leqslant 0. \end{cases} \tag{48}$$

And

$$\overrightarrow{v^{-}_{3D,blocking}} = \begin{cases} \overrightarrow{v^{-}_{r,3D}}, & if \left(\overrightarrow{v^{-}_{r,3D}} \times \overrightarrow{v^{-}_{m,3D}}\right) \cdot \overrightarrow{n_r} < 0; \\ \overrightarrow{v^{-}_{m,3D}}, & if \left(\overrightarrow{v^{-}_{r,3D}} \times \overrightarrow{v^{-}_{m,3D}}\right) \cdot \overrightarrow{n_r} \geqslant 0. \end{cases} \tag{49}$$

To take into account the shading:

$$\overrightarrow{v^{+}_{3D}} = \overrightarrow{v^{+}_{3D,shading/blocking}} = \begin{cases} \overrightarrow{v^{+}_{3D,blocking}}, & if \left(\overrightarrow{v^{+}_{3D,blocking}} \times \overrightarrow{v^{+}_{m,3D,reflection}}\right) \cdot \overrightarrow{n_r} > 0; \\ \overrightarrow{v^{+}_{m,3D,reflection}}, & if \left(\overrightarrow{v^{+}_{3D,blocking}} \times \overrightarrow{v^{+}_{m,3D,reflection}}\right) \cdot \overrightarrow{n_r} \leqslant 0. \end{cases} \tag{50}$$

And

$$\overrightarrow{v^{-}_{3D}} = \overrightarrow{v^{-}_{3D,shading/blocking}} = \begin{cases} \overrightarrow{v^{-}_{3D,blocking}}, & if \left(\overrightarrow{v^{-}_{3D,blocking}} \times \overrightarrow{v^{-}_{m,3D,reflection}}\right) \cdot \overrightarrow{n_r} < 0; \\ \overrightarrow{v^{-}_{m,3D,reflection}}, & if \left(\overrightarrow{v^{-}_{3D,blocking}} \times \overrightarrow{v^{-}_{m,3D,reflection}}\right) \cdot \overrightarrow{n_r} \geqslant 0. \end{cases} \tag{51}$$

The acceptance angles incorporating blocking and shading in three dimensions can then be calculated as:

$$\beta^{+,k}_{3D}(x,z) = \arccos\left(\frac{\overrightarrow{v^{+}_{3D}} \cdot \overrightarrow{v_n}}{\left|\overrightarrow{v^{+}_{3D}}\right| \cdot \left|\overrightarrow{v_n}\right|}\right);$$

$$\beta^{-,k}_{3D}(x,z) = \arccos\left(\frac{\overrightarrow{v^{-}_{3D}} \cdot \overrightarrow{v_n}}{\left|\overrightarrow{v^{-}_{3D}}\right| \cdot \left|\overrightarrow{v_n}\right|}\right). \tag{52-53}$$

3.6. Calculation of intercept factor

For the point (x,z) on the mirror k, the local intercept factor can be calculated as:

$$\gamma^{k,local}(x,z) = \int_{\beta^{-,k}_{3D}(x,z)}^{\beta^{+,k}_{3D}(x,z)} g_{eff}(\beta)d\beta. \tag{54}$$

Integration of $\boldsymbol{\gamma^{k,local}(x,z)}$ over the mirror k aperture yields the intercept factor for the mirror k:

$$\gamma^{k} = \frac{1}{w^{k} \cdot \cos(\tau^{k} - \theta_{\perp})} \cdot \int_{-x^{k}_{1}}^{x^{k}_{2}} \gamma^{k,local}(x,z(x))dx. \tag{55}$$

Here, $\boldsymbol{z = z(x)}$ defines the shape of the mirror k in the transversal plane. The term $\boldsymbol{\cos(\tau^{k} - \theta_{\perp})}$ accounts for the cosine effect of the inclined mirror k relative to the incoming sun ray direction.

The intercept factor for the overall linear Fresnel collector including n mirrors can be obtained by combining the individual intercept factor of each mirror:

$$\gamma(\theta_{\perp},\theta_{\parallel}) = \frac{\sum_{k=1}^{n}(\gamma^{k} \cdot w^{k})}{\sum_{k=1}^{n}(w^{k})}. \tag{56}$$

3.7. Optical efficiency, intercept factor, and incidence angle modifier

The optical efficiency of a collector is used to measure its optical performance before taking into account heat loss between the solar receiver and the ambient. It can be expressed as (Bendt et al., 1979):

$$\eta = \gamma\rho\tau\alpha. \tag{57}$$

Here, ρ is the reflector reflectance; τ is the transmittance of the receiver glass envelope (if applicable); and α is the average absorptance of the receiver surface. ρ, τ, and α are optical properties of the materials used in the collector, and they are a function of incidence angle to the material surface.

The optical efficiency varies with the sun position and is a function of incidence angle, $(\theta_{\perp},\theta_{\parallel})$. The incidence angle modifier (IAM) is then a function of both the transversal incidence angle $\theta_{\perp}$ and the longitudinal incidence angle $\theta_{\parallel}$. Assuming the IAM accounts for the cosine effect of varying incidence angle on the intercept area of the collector aperture, the optical efficiency at any incidence angle can then be calculated as:

$$\eta(\theta_{\perp},\theta_{\parallel}) = \eta_{0} \cdot IAM(\theta_{\perp},\theta_{\parallel}). \tag{58}$$

Here, η_0 is the optical efficiency at normal incidence (i.e., $\theta_{\perp} = \theta_{\parallel} = 0$).

Assuming the optical properties of the materials (ρ, τ, and α) do not change with varying incidence angle, the correlation between intercept factor and IAM becomes:

$$IAM(\theta_{\perp},\theta_{\parallel}) = \gamma(\theta_{\perp},\theta_{\parallel})/\gamma_{0}. \tag{59}$$

Here, γ_0 is the intercept factor at normal incidence.

For computational convenience, the incidence angle modifier is often factorized into two individual functions:

$$IAM(\theta_{\perp},\theta_{\parallel}) \cong IAM_{t}(\theta_{\perp}) \cdot IAM_{l}(\theta_{\parallel}). \tag{60}$$

4. Validation

A suite of MATLAB code was developed based on the detailed mathematical model above. To validate the First-OPTIC approach, two sets of test cases are performed and compared with ray-tracing results.

4.1. Geometric errors

First, three cases are set up to test the capability of First-OPTIC to evaluate geometric errors. The linear Fresnel collector used for validation includes 18 rows of parabolic mirrors with a width of 0.75 m and a uniform spacing of 1.2 m, and two virtual receivers with a diameter of 0.07 m, a spacing 0.07 m along the x axis, and a height

of 8 m. The center of the two receivers is located at (0, 0, 8), referring to the coordinates shown in Fig. 1. Three different optical/geometric error scenarios are designed to test each individual geometric error: mirror slope error, mirror tracking error, and receiver position error, as shown in Table 1.

The ray-tracing software SolTrace (Wendelin, 2003) is used to provide ray-tracing results for the test cases. SolTrace is a Monte-Carlo ray-tracing tool developed for solar concentrator applications. It has been proven to provide accurate optical evaluation for a variety of solar concentrating applications (Wendelin, 2003). Table 2 summarizes the calculation results of intercept factors at normal incidence by employing FirstOPTIC and SolTrace. For cases I and II, due to the fact that the collector is at normal incidence and the slope or tracking error is constant, there is equivalent probability distribution to represent the slope/tracking error as part of the effective beam spread, as given in Eq. (2). In particular, the constant slope error $\varepsilon_x = 2$ mrad is equivalent to a probability distribution function represented by a Dirac delta function:

$$\delta_{slope}(\beta) = \begin{cases} +\infty, & \beta = 4 \text{ mrad} \\ 0, & \beta \neq 4 \text{ mrad} \end{cases} \tag{61}$$

Note that a factor of 2 is applied to the conversion above, similar to Eq. (4). In case II, the tracking error $\Delta\tau = 1$ mrad is also equivalent to a Dirac delta function, which can then be convolved with the effective beam spread function (5):

$$\delta_{tracking}(\beta) = \begin{cases} +\infty, & \beta = 2 \text{ mrad} \\ 0, & \beta \neq 2 \text{ mrad} \end{cases} \tag{62}$$

An equivalent conversion does not exist for the receiver position error in case III. The approach employing the equivalent error probability distributions is denoted as FirstOPTIC (optical-equivalent) in Table 2. Because FirstOPTIC (optical-equivalent) simply uses the effective beam spread function and does not require any geometric modification for mirror surface or orientation, it stands as the reference solution for comparison with cases I and II.

Table 2 shows a comparison of the results using FirstOPTIC and SolTrace. There is good agreement between the two approaches for the intercept factor calculation for all three cases. In general, FirstOPTIC is much faster than SolTrace due to its analytical nature: FirstOPTIC integrates the effective beam spread over the angular range intercepted by the receiver as a whole, while SolTrace has to trace every single sun ray passing through the system. Mathematically, SolTrace involves a higher order of intensive computing than FirstOPTIC. For cases II and III, it takes about 33 s for SolTrace (1 million rays used), compared with about 3 s for FirstOPTIC, while maintaining roughly the same level of accuracy. For Case I, when mirror surface slope error is applied as a geometric modification to the surface slope, SolTrace takes much longer than FirstOPTIC: about 3768 s for SolTrace compared to about 3 s for FirstOPTIC. This is because every time a sun ray is traced through the collector system, the local mirror surface needs to be reconstructed through discrete points representing the mirror surface and its geometric error. Local surface reconstruction could be very time consuming and inaccurate in many cases (Zhu et al., 2006). However, it should be noted that SolTrace can provide a solar flux map for the receiver surface, which FirstOPTIC cannot do.

4.2. Cases with non-zero incidence angles

Next, test cases with non-zero incidence angles are generated for further validation. In Fig. 5, the intercept factors as a function of the transversal and longitudinal incidence angle are plotted for the test linear Fresnel collector using FirstOPTIC and SolTrace. The test collector includes 10 rows of parabolic mirrors with a width of 0.75 m and a uniform spacing of 1.2 m, and a single circular virtual receiver with a diameter of 0.09 m and a height of 8 m. The sun shape is defined by a Gaussian with a RMS of 2.8 mrad. The optical error is simply another Gaussian with a RMS of 5.0 mrad. The overall effective beam spread will be the convolution of the sun shape and the optical error. As seen from the figure, the results of the two approaches match very well for a wide range of transversal and longitudinal incidence angles, $0° \sim 85°$. The largest absolute errors of the intercept are 0.020 for the transversal and 0.015 for the longitudinal incidence angle.

Fig. 6 shows a comparison of the results for a test linear Fresnel collector that includes multiple receivers. The test collector is composed of 18 mirrors with a width of 0.75 m and a uniform spacing of 1.2 m, and two virtual receivers with a diameter of 0.07 m, a spacing of 0.07 m, and a height of 8 m. The sun shape and the optical error are same as in the previous case. The comparison between FirstOPTIC and Soltrace is given in the figure. It is shown that the intercept factors calculated by the two approaches give rise to very little difference. The largest absolute errors between FirstOPTIC and SolTrace are 0.010 for the transversal and 0.018 for the longitudinal incidence angle.

Table 1
Test cases for the linear Fresnel collector at normal incidence.

Cases	Optics		Geometric Errors		
	Sun shape	Mirror specularity	Slope error	Tracking error	Receiver position error
I	*Gaussian:* $\sigma = 2.8$ mrad	*Gaussian:* $\sigma = 0.8$ mrad	*Constant:* $\varepsilon_x = 2$ mrad	*None*	*None*
II	*Gaussian:* $\sigma = 2.8$ mrad	*Gaussian:* $\sigma = 0.8$ mrad	*None*	$\Delta\tau = 1$ mrad	*None*
III	*Gaussian:* $\sigma = 2.8$ mrad	*Gaussian:* $\sigma = 0.8$ mrad	*None*	*None*	$\Delta z = -0.035$ *m.*

Table 2
Comparison of results for intercept factor using various approaches.

		FirstOPTIC (Optical-equivalent)	FirstOPTIC (Geometric)	SolTrace (Geometric)
Case I	Intercept factor	0.7452	0.7452	0.7475
	Error	–	0.00%	0.3%
	Time (seconds)	3.05	3.10	3768[a]
Case II	Intercept factor	0.8596	0.8597	0.8639
	Error	–	0.01%	0.5%
	Time (seconds)	3.06	3.09	33.63
Case III	Intercept factor	–	0.8638	0.8678
	Error	–	–	–
	Time (seconds)	–	3.12	32.87

[a] *Note*: 0.1 million rays were used to solve Case I using SolTrace.

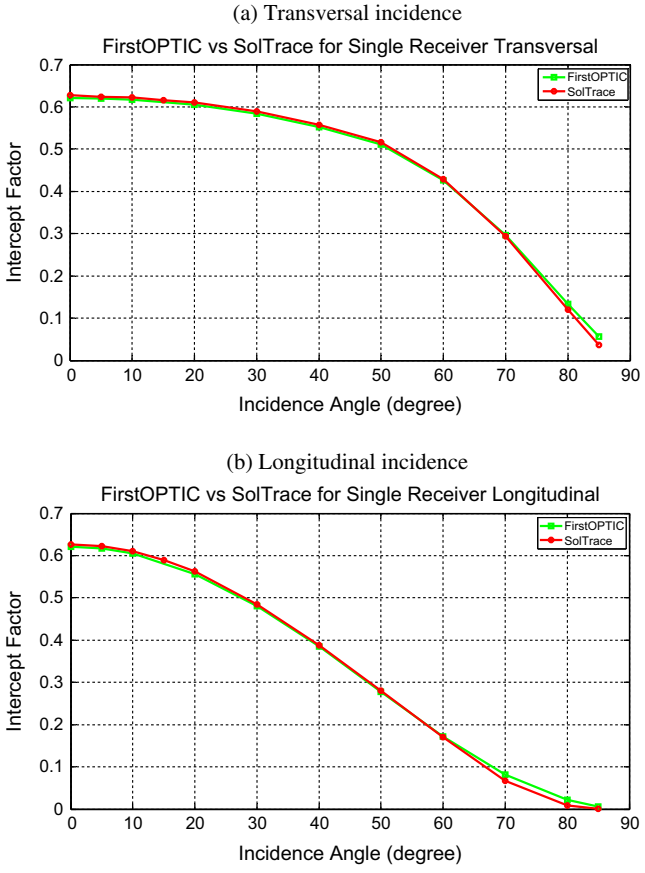

Fig. 5. Comparison of intercept factor as a function of incidence angle between FirstOPTIC and SolTrace for single-receiver collectors.

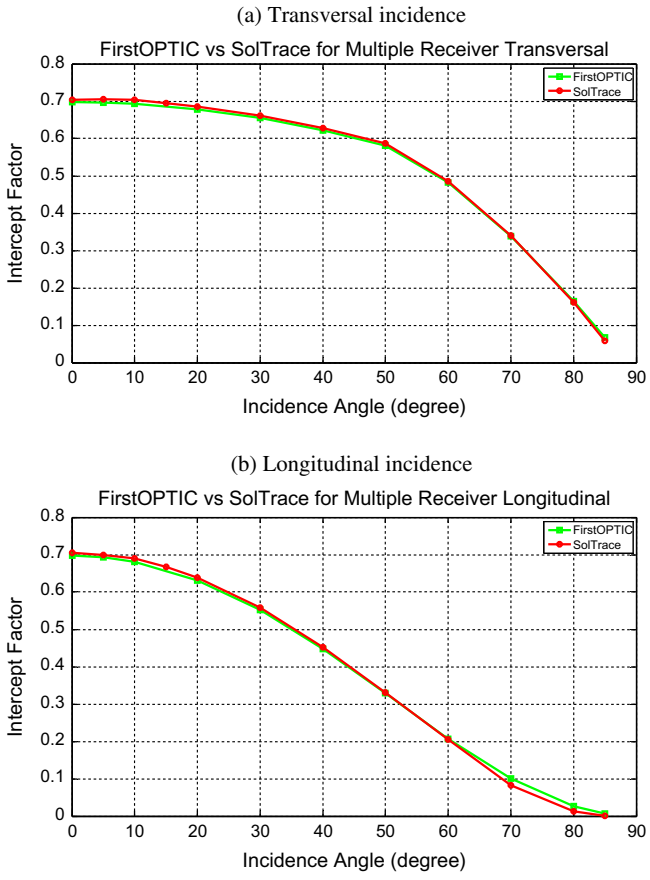

Fig. 6. Comparison of intercept factor as a function of incidence angle between FirstOPTIC and SolTrace for two-receiver collectors.

5. Case Study

After validation of the FirstOPTIC method, it is then applied to study the calculation error when the IAM is factorized into two independent components: the transversal and longitudinal, as defined in Eq. (60). The two-receiver collector in the section above is used along with the same sun shape profile and the optical error. In Fig. 7, (a) presents the IAM as a coupled function of both transversal and longitudinal incidence angles, while (b) gives the IAM as a factorized function of the transversal and longitudinal incidence angle, respectively. All the IAMs are calculated using the developed FirstOPTIC code. For the coupled IAM representation, each IAM was calculated for each set of transversal and longitudinal incidence angles; for the factorized IAM representation, the IAM as a function of the transversal or longitudinal incidence angle is calculated when the longitudinal or transversal incidence angle is zero.

The error resulting from the IAM factorization (Eq. (60)) is calculated against the coupled IAM function and plotted in Fig. 8. It is seen that the error is small in general and less than 0.05: the error of factorized IAM is minimal

(a) IAM as a coupled function of transversal and longitudinal incidence angles

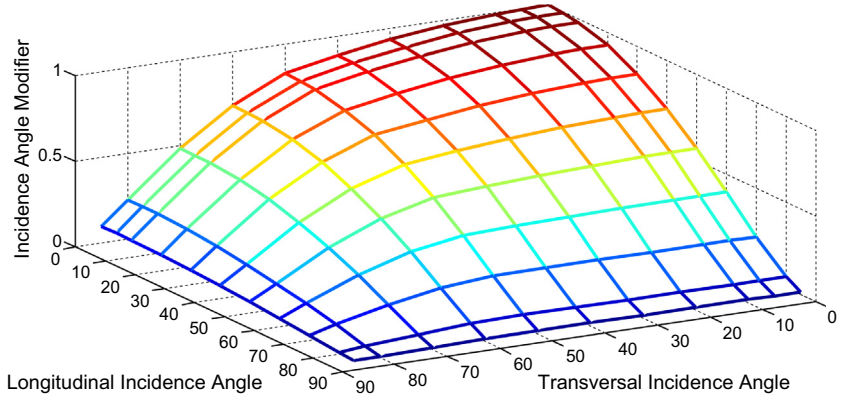

(b) IAM as a factorized function of transversal and longitudinal incidence angles

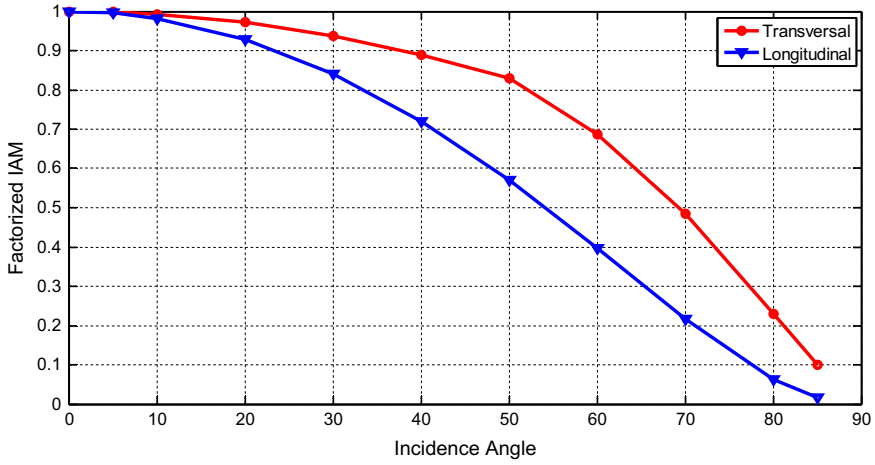

Fig. 7. Two representations of IAM as a function of incidence angle.

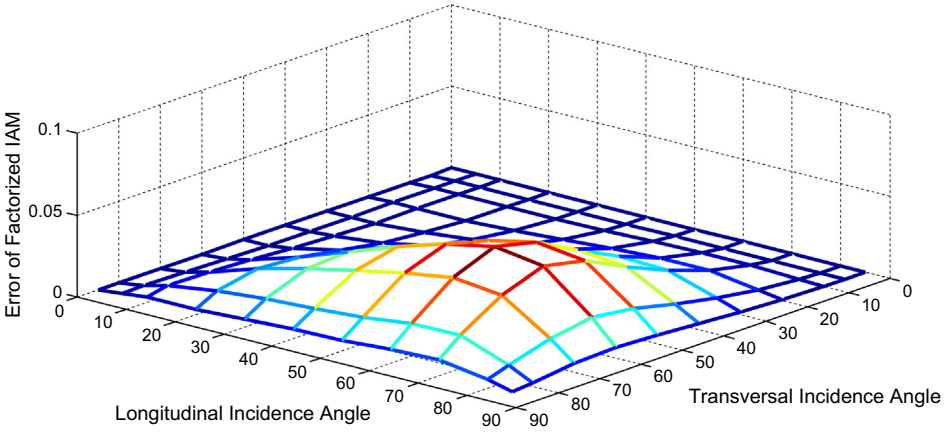

Fig. 8. Error of factorized IAM representation.

when either transversal or longitudinal incidence angle is small, while the error is relatively large when both incidence angles are moderate. The largest absolute error is about 0.05 for the case studied here. It is worth pointing out that the factorized IAM can be a very accurate approximation but generally underestimates the intercept factor when compared to the coupled IAM representation.

6. Conclusions

In this paper, an analytical approach—FirstOPTIC—is developed and implemented as a suite of MATLAB code for linear Fresnel collectors. The FirstOPTIC approach has been carefully validated and it is shown that FirstOPTIC can provide accurate calculation of intercept factor

and exhibit outstanding advantages in computing speed compared to a ray-tracing approach.

FirstOPTIC is particularly suitable for design and optimization of linear Fresnel technology involving a large number of collector design options. In addition, it is also designed for detailed optical analysis involving a large volume of optical and/or mechanical characterization data and can be a very valuable tool in the collector prototyping stage as well. In addition, the FirstOPTIC approach can be naturally extended to central-receiver towers.

At the same time, there are also a few limitations on the developed FirstOPTIC. First of all, FirstOPTIC is an analytical approach to characterize geometrical optics of a solar collector. The variation of material optical properties such as mirror reflectance and absorber absorptance as a function of incidence angle (Montecchi, 2012; Nicodemus et al., 1977) is not accounted into the FirstOPTIC approach yet. Secondly, the developed FirstOPTIC is limited to linear Fresnel collectors without secondary reflectors. In the future, FirstOPTIC may be enhanced with the capability to analyze secondary reflectors and incorporating variations of optical properties of collector components.

Acknowledgement

This work was supported by the U.S. Department of Energy under Contract No. DE-AC36-08GO28308 with the National Renewable Energy Laboratory (NREL).

References

Andraka, C., Sadlon, S., Myer, B., Trapeznikov, K., Liebner, C., 2009. SOFAST: sandia optical fringe analysis slope tool for mirror characterization. In: SolarPACES 2009, Berlin, Germany.

Barale, G., Heimsath, A., Nitz, P., Toro, A., 2010. Optical design of a linear fresnel collector for sicily. In: 16th SolarPACES International Symposium Perpignan, France.

Bendt, P., Rabl, A., Gaul, H.W., Reed, K.A., 1979, Optical Analysis and Optimization of Line Focus Solar Collectors. No. SERI/TR-34-092, SERI, Golden, CO, USA.

Bernhard, R., Laabs, H.G., de Lalaing, J., Eck, M., Eickhoff, M., Pottler, K., Morin, G., Heimsath, A., Georg, A., and Haberle, A., 2008. Linear Fresnel collector demonstration on the PSA Part I – Design: construction and quality control. In: 15th SolarPACES International SymposiumBerlin, Germany.

Binotti, M., Zhu, G., Gray, A., Manzolini, G., Silva, P., 2013. Geometric analysis of three-dimensional effects of parabolic trough collectors. Solar Energy, 88.

Boas, M.L., 1983. Mathematical Methods in the Physical Sciences. John Wiley and Sons Ltd..

Breault Research Organization. <http://www.breault.com/software/asap.php>.

Brost, R., Zhu, G., 2009. Commercial Development of an Advanced, High-Temperature, Linear-Fresnel Based Concentrating Solar Power Concept. SkyFuel, Prepared under DOE FOA No. DE-FC36-08GO18034.

Brost, R., Zhu, G., 2010. Design of a High-Temperature Molten Salt Linear Fresnel Collector. <http://www1.eere.energy.gov/solar/review_meeting/pdfs/prm2010_skyfuel.pdf>.

Conlon, W.M., 2011. Superheated steam from CLFR solar steam. In: 17th SolarPACES International SymposiumGranada, Spain.

Gee, R., Brost, R., Zhu, G., Jorgensen, G., 2010. An improved method for characterizing reflector specularity for parabolic concentrators. In: 16th SolarPACES, Perpignan, France.

Kolb, G., Jones, S.A., Donnelly, M., Gorman, D., Thomas, R., Davenport, R., Lumia, R., 2007. Heliostat Cost Reduction Study, Sandia National Laboratories, Albuquerque, NM.

Meyen, S., Montecchi, M., Kennedy, C., Zhu, G., Gray, M., et al., 2013. Parameters and Method to Evaluate the Solar Reflectance Properties of Reflector Materials for Concentraing Solar Power Technology Draft Version 2.4, SolarPACES.

Mills, D., Morrison, G., 2000. Compact linear Fresnel reflector solar thermal power plants. Solar Energy 68 (3), 262–283.

Montecchi, M., 2012. Approximated method for modeling hemispherical reflectance and evaluating near-specular reflectance of CSP mirrors. In: The SolarPACES 2012Marrakech, Morocco.

Morin, G., Mertins, M., Kirchberger, J., Selig, M., 2011. SuperNOVA-construction, control & performance of steam superheating linear fresnel collector. In: 17th SolarPACES International SymposiumGranada, Spain.

Nicodemus, F.E., Richmond, J.C., Hsia, J.J., Ginsberg, I.W., Limperis, T., 1977. Geometrical Considerations and Nomenclature for Reflectance. National Bureau of Standards, Dpeartment of Commerce.

Pettit, R.B., 1977. Characterization of the reflected beam profile of solar mirror materials. Solar Energy 19, 733–741.

Pottler, K., Lupfert, E., Johnston, G., Shortis, M., 2005. Photogrammetry: a powerful tool for geometric analysis of solar concentrators and their components. Journal of Solar Energy Engineering 127 (1), 94–101.

Price, H., Lupfert, E., Kearney, D., Zarza, E., Cohen, G., Gee, R., Mahoney, R., 2002. Advances in parabolic trough solar power technology. Journal of Solar Energy Engineering 124 (2), 109–125.

Rabl, A., 1976. Comparison of solar concentrators. Solar Energy 18, 93.

Rabl, A., 1985. Active Solar Collectors and Their Applications. Oxford University Press, New York.

Selig, M., 2011. Commercial CSP based on Fresnel collector technology. In: 17th SolarPACES International SymposiumGranada, Spain.

Wendelin, T., 2003. SolTrace: a new optical modeling tool for concentrating solar optics. In: 2003 International Solar Energy Conference, Hawaii, USA.

Wendelin, T., May, K., Gee, R., 2006. Video scanning hartmann optical testing of state-of-the-art parabolic trough concentrators. In: Solar 2006 Conference, Denver, Colorado USA.

Zhu, G., 2013. Study on the optical impact of receiver position error on parabolic trough collectors. Journal of Solar Energy Engineering (in press).

Zhu, G., Lewandowski, A., 2012. A new optical evaluation approach for parabolic trough collectors: first-principle OPTical Intercept Calculation (FirstOPTIC). Journal of Solar Energy Engineering, 134.

Zhu, G., Mammoli, A., Power, H., 2006. A 3-D indirect boundary element method for bounded creeping flow of drops. Engineering Analysis with Boundary Elements 30, 856–868.

Zhu, G., Wendelin, T., Wagner, M., Kutscher, C., 2013. History, current-state and future of linear Fresnel concentrating solar collectors. Solar Energy (accepted for publication).